Towards Template-Assisted Assembly of Nematic Colloids

Nuno M. Silvestre,[1,2] Qingkun Liu,[3] Bohdan Senyuk,[3] Ivan I. Smalyukh,[3,4,5,6] and Mykola Tasinkevych[7,8,*]
[1]Departamento de Física da Faculdade de Ciências, Universidade de Lisboa, Avenida Professor Gama Pinto 2, P-1649-003 Lisboa, Portugal
[2]Centro de Física Teórica e Computacional, Universidade de Lisboa, Avenida Professor Gama Pinto 2, P-1649-003 Lisboa, Portugal
[3]Department of Physics, University of Colorado, Boulder, Colorado 80309, USA
[4]Liquid Crystal Materials Research Center, University of Colorado, Boulder, Colorado 80309, USA
[5]Department of Electrical, Computer, and Energy Engineering and Materials Science and Engineering Program, University of Colorado, Boulder, Colorado 80309, USA
[6]Renewable and Sustainable Energy Institute, National Renewable Energy Laboratory and University of Colorado, Boulder, Colorado 80309, USA
[7]Max-Planck-Institut für Intelligente Systeme, Heisenbergstrasse 3, D-70569 Stuttgart, Germany
[8]Institut für Theoretische Physik IV, Universität Stuttgart, Pfaffenwaldring 57, D-70569 Stuttgart, Germany
(Received 16 March 2014; published 2 June 2014)

Colloidal crystals belong to a new class of materials with unusual properties in which the big challenge is to grow large-scale structures of a given symmetry in a well-controlled and inexpensive way. Recently, template-assisted crystallization was successfully exploited experimentally in the case of colloidal particles dispersed in isotropic fluids. In liquid crystal (LC) colloids, particles are subjected to long-range anisotropic elastic forces originating from the anisotropic deformation of the underlying order parameter. These effective interactions are easily tunable by external electric or magnetic fields, light, temperature, or confinement and, thus, provide additional handles for better control of colloidal assembly. Here we use the coupling between microsculptured bounding surfaces and LC elasticity in order to guide the self-assembly of large-scale colloidal structures. We present explicit numerical calculations of the free energy landscape of colloidal particles in the presence of convex protrusions modeled as squared pyramids comparable to the size of the particles. We show the existence of strong trapping potentials that are able to efficiently localize the colloidal particles and withstand thermal fluctuations. Three-dimensional optical imaging experiments support the theoretical predictions.

DOI: 10.1103/PhysRevLett.112.225501 PACS numbers: 81.16.Dn, 81.05.Xj, 82.70.Dd, 83.80.Xz

Colloidal crystals are periodic structures formed typically by micron-sized particles, with the lattice periodicity comparable to the wavelength of visible light. In this way, colloidal crystals can be used to control and manipulate the behavior of light, for example, as photonic band-gap crystals [1]. Conventional approaches to grow large-scale three-dimensional colloidal crystals fall into three main classes [2]: (i) sedimentation in a gravitational field, where the crystalline order is enhanced by external stimuli (e.g., shearing [3]), (ii) crystallization through repulsive electrostatic interactions, and (iii) self-assembly under strong physical confinement. Controlling the symmetry and orientation of the colloidal crystals is crucial for the development of electronic devices and photonic band-gap crystals and can be achieved through template-assisted colloidal assembly [4,5]. This method relies on topographically patterned substrates as a template to drive the nucleation and epitaxial growth of colloidal structures. The topography acts as an ordering external field and can be tuned using conventional microfabrication techniques such as soft lithography [6].

Given their unique mechanical and electro-optical properties, liquid crystal (LC) colloids have been proposed as promising candidates for photonic crystals. Their long-range colloid-colloid interactions guide the aggregation of colloidal particles, which are stabilized by short-distance repulsions resulting from the presence of topological defects [7,8] and strongly depend on the properties of the LC host, on the size shape, and the surface properties of the particles [9–14]. Typically, colloidal particles in LCs exhibit binding potentials ranging from a few $100k_BT$ to some $1000k_BT$, which stabilizes the colloidal assemblies against thermal fluctuations [15–18]. Two-dimensional (2D) [16] or three-dimensional (3D) [18] colloidal crystallites composed of $\sim$100 particles were recently assembled with the help of optical manipulation. This technique, although useful from the basic point of view, is not so efficient from the viewpoint of application because it requires a human intervention at each step of the assembly process. A promising alternative for obtaining large 3D colloidal structures in LCs is to pattern the LC environment by using, e.g., external electric fields or bounding surfaces. Recently, the defect-assisted assembly of colloidal particles trapped at LC-fluid interfaces was demonstrated [19,20].

In this Letter, we analyze in detail, both experimentally and theoretically, the efficiency of sculptured surfaces as templates for self-assembly in LC colloids. With the aid of

3D imaging of the director field [21,22] and theoretical analysis based on the numerical minimization of the Landau–de Gennes free energy [23], we demonstrate that a properly patterned bounding surface modulates the LC environment acting as an effective external ordering potential upon dispersed colloidal particles. To minimize the elastic free energy of the LC medium, particles preferably position themselves close to the regions of maximal distortions, i.e., close to nonuniformities of the substrate. Our results provide new insights into how the interplay between the relief of a confining surface and the LC elasticity can be used in practical applications.

Substrates patterned by concave features (i.e., roughly speaking, by holes) can efficiently trap particles employing self-complementary key-lock mechanisms enhanced by LC elasticity [24]. Although such surfaces could be used as templates for colloidal crystallization, they are not robust enough because only particles with the right geometrical parameters may be targeted by concave patterns; moreover, they are basically patterns of a single use only. Indeed, due to van der Waals, or depletion forces, colloidal particles get irreversibly trapped within the substrate cavities. Therefore, here we follow an alternative route and target topological defects, instead of the particles themselves, with the extra advantage that upon melting the LC medium, the particles would diffuse away from their trapping spots. This can be achieved by using convex protrusions, which are modeled here as square pyramids (Fig. 1).

In the experiments, we used silica particles (SPs) of diameter $2R = 3.14$ μm (Bangs Laboratories, Inc.) treated with a water solution of DMOAP [dimethyloctadecyl [3-(trimethoxysilyl) propyl] ammonium chloride, Sigma-Aldrich] for strong homeotropic anchoring and melamin resin (MR) particles of diameter $2R = 3$ μm (Fluka) promoting tangential degenerate anchoring of LC [25]. Colloidal particles were dispersed in a nematic material 5CB (4-pentyl-4-cyanobiphenyl from Frinton Laboratories, Inc.). Colloidal nematic dispersions were confined between two thin glass substrates, one of which was patterned with arrays of pyramids [Figs. 2(a), 2(b), and 2(d)]. Pyramids were produced by curing UV epoxy (NOA 65, Norland Products, Inc.) between a glass substrate and the pyramid template and peeling it off from the template. A pyramid template was fabricated by photolithographic patterning 5 μm × 5 μm squares on photoresist by a mask and chemically anisotropic etching of single-crystal silicon substrates [26]. The pyramids and colloids of comparable sizes were considered to avoid situations when more than one particle could enter into the potential well close to the pyramid tip. Epoxy pyramids as made promote tangential anchoring of 5CB. To induce homeotropic anchoring, epoxy pyramids were additionally treated with oxygen plasma for 10 min and then DMOAP solution. Glass substrates were treated with DMOAP for homeotropic anchoring and polyimide PI2555 (HD Microsystem) was spin coated, baked, and rubbed unidirectionally for homogeneous alignment. We used an inverted microscope (Olympus IX81) for optical

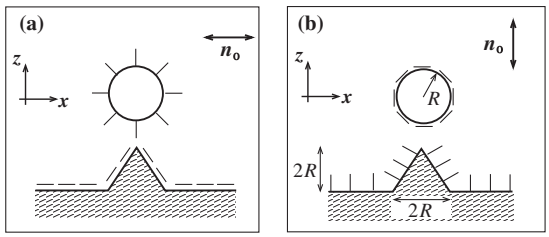

FIG. 1. Schematic illustrations of a spherical colloidal particle of the radius R in the vicinity of a convex protrusion modeled as a pyramid with the square base of length $2R$ and height $2R$. (a) Homeotropic anchoring at the particle's surface (SP in the experiments) and tangential degenerate anchoring at the substrate. The far-field director $\mathbf{n}_0$ is parallel to the x axis. (b) Tangential degenerate anchoring at the surface of the colloidal particle (MR in the experiments) and homeotropic anchoring at the substrate. $\mathbf{n}_0$ is along the z axis.

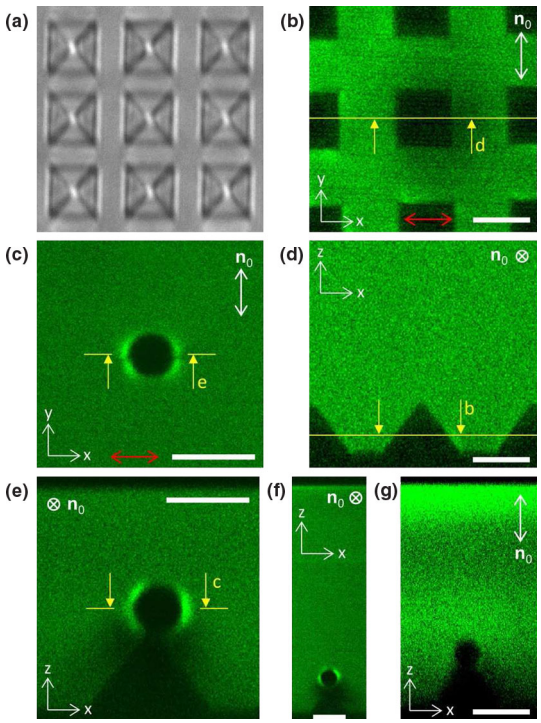

FIG. 2 (color online). Experimental textures of particles elastically trapped at the tip of the pyramids patterned at the glass substrate: unpolarized bright field (a) and 3PEF-PM in-plane xy (b) and cross sectional zx (d) textures of a substrate patterned with a pyramid array in a planar liquid crystal cell. (c) SP with homeotropic anchoring and a Saturn ring defect elastically trapped on the tip of a pyramid with planar anchoring in the thin (e) and thick (f) nematic cell. (g) MR particle with tangential degenerate anchoring elastically trapped on the tip of a pyramid with homeotropic anchoring. White double arrow and crossed circle show a far-field director $\mathbf{n}_0$, respectively, in plane and out of plane of the image. Dark red double arrow shows the direction of the polarization of excitation beam. Scale bar is 5 μm.

observations, laser manipulations, and 3D imaging of a director field [21,22]. Laser manipulations with colloids were performed at a wavelength of 1064 nm, and a laser beam at 870 nm was used for excitation of 5CB in 3D three-photon excitation fluorescence polarizing (3PEF-PM) imaging [21,22].

The theoretical description is based on numerical minimization of the Landau–de Gennes free energy functional [23], whose density consists of the bulk $f_b = a_o(T-T^*)Q_{ij}^2 - bQ_{ij}Q_{jk}Q_{ki} + c(Q_{ij}^2)^2$ and elastic $f_e = (L_1/2)(\partial_k Q_{ij})^2 + (L_2/2)\partial_j Q_{ij}\partial_k Q_{ik}$ terms. Here, $Q_{ij}, (i,j=1,2,3)$ is a traceless symmetric tensor order parameter, and summation over repeated indexes is implied. a_0, b, c, L_1, L_2 are phenomenological material-dependent parameters, T is the temperature, and T^* is the supercooling temperature of the isotropic phase. Homeotropic confining surfaces are taken into account by the following surface free energy density $f_s^{\perp} = W(Q_{ij} - Q_{ij}^s)^2$, where W is the anchoring strength, and Q_{ij}^s is the surface preferred order parameter. Surfaces imposing planar degenerate anchoring are described by surface potential [27] $f_s^{\parallel} = W((\tilde{Q}_{ij} - \tilde{Q}_{ij}^{\perp}) + (\tilde{Q}_{ij}^2 - 3Q_b^2/2)^2)$, where W controls the anchoring strength, $\tilde{Q}_{ij} \equiv Q_{ij} + Q_b\delta_{ij}/2$, $\tilde{Q}_{ij}^{\perp}$ is the projection of $\tilde{Q}_{ij}$ onto the confining surface, and Q_b is the bulk value of the scalar order parameter (see the Supplemental Material [28]). We introduce a dimensional anchoring strength $w = WQ_b^2R/K$, where K is the average Frank elastic constant and use the following values of the model parameters: $a_0 = 0.044 \times 10^6$ J/Km^3, $b = 0.816 \times 10^6$ J/m^3, $c = 0.45 \times 10^6$ J/m^3, $T^* = 307$ K, $L_1 = 6 \times 10^{-12}$ J/m, $L_2 = 12 \times 10^{-12}$ J/m (these are typical values for 5CB [36]). Then the total free energy functional $F = \int_V dv(f_b + f_e) + \int_{\partial V} dsf_s$ is minimized numerically by using finite elements methods with adaptive meshing, as described in the Supplemental Material [28] and in more detail in Ref. [17].

Figure 1 schematically summarizes the system geometry considered here. We considered two cases: planar degenerate substrate (homeotropic colloid) and homeotropic substrate (planar degenerate colloid). The cases of like anchoring types at the substrates and particles are not optimal, because in these cases, colloidal particles get trapped in the wedgelike region at the bases of the pyramids. On the other hand, colloidal particles with anchoring different from that of the substrate are attracted to the pyramid tips. The SP colloids in planar cells induced quadrupolar distortions with a singular disclination loop [Fig. 2(c)] known as a Saturn ring [14]. They were elastically trapped at the tip of the pyramids with tangential anchoring [Figs. 2(e) and 2(f)], similar to simulated textures [Figs. 3(c) and 3(d)]. MR particles dispersed in a nematic LC induce elastic quadrupoles with two surface point defects (called boojums) at their poles. Some of the MR particles in nematic homeotropic cells were spontaneously trapped at the tip of the pyramids with homeotropic anchoring [Fig. 2(g)], similar to simulated

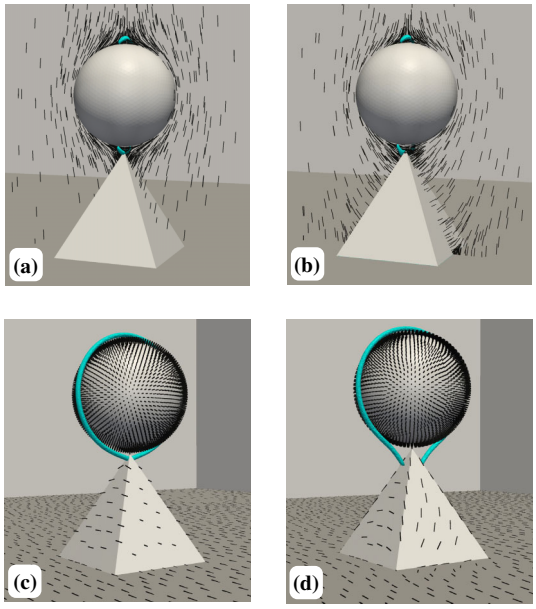

FIG. 3 (color online). Colloidal particles trapped at the tips of pyramidlike protrusions: the centers of the colloidal particles and the pyramid tips are aligned in the vertical direction. The surface-to-surface distance d from the tips to the particles $d = 0.1R$. (a), (b) Strong ($w_{\mathrm{col}} = 22$) planar degenerate anchoring is assumed at the surface of the particle with homeotropic anchoring at the patterned substrate. (c),(d) Strong homeotropic anchoring at the particle surface and planar degenerate anchoring at the substrate. Regimes of a neutral ($w_{\mathrm{sub}} = 0$), (a),(c), and strong ($w_{\mathrm{sub}} = 22$) anchoring (b),(d) substrates are presented. Numerically calculated $\mathbf{n}(\mathbf{r})$ is shown by short black lines. Isosurfaces of reduced scalar order parameter $Q = 0.5Q_b$ are shown in blue color. The sharp edges of the pyramids also induce a reduction of the local orientational order but correspond to regions where $Q > 0.5Q_b$; hence, they are not represented here.

textures [Figs. 3(a) and 3(b)]. Although the particles were trapped at the tip of the pyramids, as the numerical calculations revealed (Fig. 3), sometimes we also observed both SP and MR particles near the tip trapped at the faces and edges of the pyramids. This off-tip trapping may be explained by the presence of surface irregularities pinning topological defects. In the case of the edges, the pinning is facilitated by the shallowness of the free energy minimum at the tip with respect to the colloidal displacements along the edges (see the Supplemental Material, Figs. S2 and S3.) In both cases, the trapping of the particles proceeds via the so-called defect-sharing mechanism [37]. Attaching the topological defect to the tips of the pyramids is a short-range effect. The main driving force that guides the particles towards the pyramids stems from the elastic deformations of the nematic director. Figure 4 shows the Landau–de Gennes free energy landscape for the case of a sphere with planar degenerate anchoring close to a homeotropic pyramid. The free energy surface reveals a bell-like shape with the width determined by the size of the pyramid base. The depth of the free energy well is $O(10^2 k_B T)$ [assuming a temperature $T = 307.2$ K, just

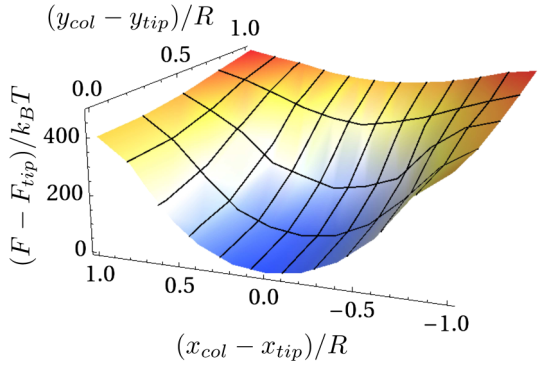

FIG. 4 (color online). Landau–de Gennes free energy F as a function of the lateral Cartesian coordinates $(x_{\mathrm{col}}, y_{\mathrm{col}})$ of the center of the particle with radius R, with planar degenerate anchoring ($w_{\mathrm{col}} = 22$) at a pyramid-decorated substrate with homeotropic anchoring ($w_{\mathrm{sub}} = 22$). The z coordinate of the colloid's center z_{col} is fixed $z_{\mathrm{col}} = z_{\mathrm{tip}} + 1.1R$. The Cartesian coordinates of the pyramid tip $(x_{\mathrm{tip}}, y_{\mathrm{tip}}, z_{\mathrm{tip}}) = (0, 0, 2R)$ and $F_{\mathrm{tip}} \equiv F(0, 0)$.

below the isotropic-nematic transition temperature, $T_{IN}(5\mathrm{CB}) = 308.5$ K]. Note also the long-range power law tails in the free energy profiles for $(x_{\mathrm{col}} - x_{\mathrm{tip}}) > R$.

The strength of the elastic interactions depends strongly on the surface anchoring energy. Decreasing the substrate anchoring strength w_{sub} by a factor of 10, the depth of the resulting trapping potential decreases from $500k_BT$ to $370k_BT$, as is shown in Fig. 5(a). The free energy profile is still long ranged and extends over several R. As expected, decreasing the anchoring strength further weakens the trapping efficiency of the pyramid. Surprisingly, at $w_{\mathrm{sub}} = 0$, the free energy depth reaches a limiting value of $50k_BT$, and the pyramid trapping range equals R. This indicates that, even for surfaces with extremely weak anchoring strength, convex protrusions still generate trapping director configurations, as is shown in Figs. 3(a) and 3(c). The inset of Fig. 5(b) shows the z component Φ_z of the force exerted upon a colloidal particle in the trapped state as a function of w_{sub}. As the anchoring strength decreases, and assuming the average Frank-Oseen elastic constant $K \sim 1$ pN, Φ_z varies in the range between 5 pN ($w_{\mathrm{sub}} \gg 1$) and 1 pN ($w_{\mathrm{sub}} \ll 1$). A similar result was obtained for the case of planar degenerate pyramids and homeotropic colloidal particles.

Recent developments in optically and thermally controlled surface topography of LC elastomer films open the possibility of further extending the scope of our template-assisted assembly of nematic colloids. Indeed, a permanent array of pyramids on one of the cell substrates that we demonstrate here can allow for the assembly of colloidal crystals of certain well-defined symmetry and geometric parameters, which can be varied by changing the template through adjusting the fabrication processes. On the other hand, similar to these pyramids cone-shaped topographic profiles in the elastomeric films can be induced, controlled, and removed by varying the temperature or through optical illumination [38–40]. Thus, potentially, template-assisted

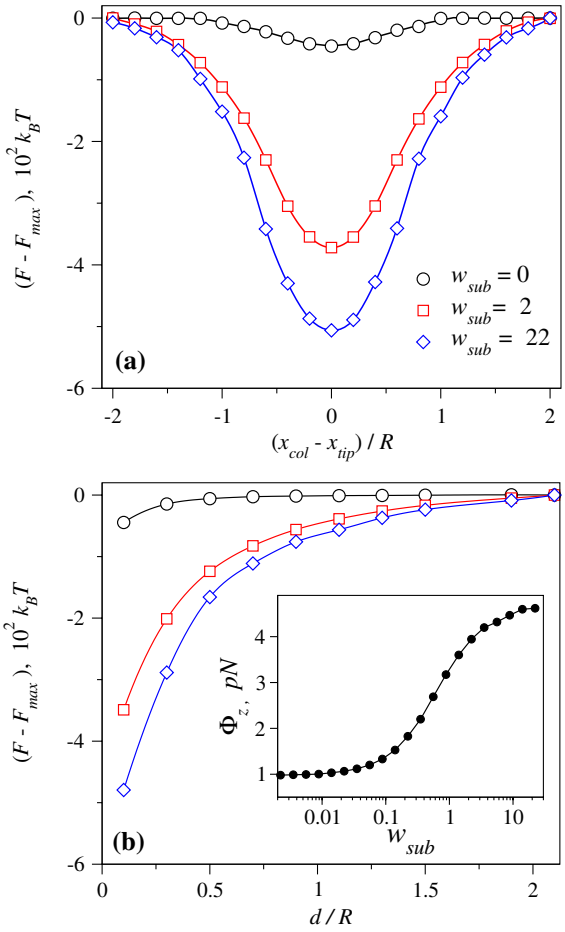

FIG. 5 (color online). Binding potential (a) as a function of x_{col} at fixed $z_{\mathrm{col}} = z_{\mathrm{tip}} + 1.1R$ and $y_{\mathrm{col}} = y_{\mathrm{tip}}$. $F_{\mathrm{max}} \equiv F(x_{\mathrm{col}} - x_{\mathrm{tip}} = 2R)$. (b) As a function of the surface-to-surface distance $d = z_{\mathrm{col}} - z_{\mathrm{tip}} - R$ to the tip of the pyramid at fixed $(x_{\mathrm{col}}, y_{\mathrm{col}}) = (x_{\mathrm{tip}}, y_{\mathrm{tip}})$ for several values of w_{sub} at the homeotropic substrate, $F_{\mathrm{max}} \equiv F(d = 2.1R)$. Inset in (b) shows the vertical component of the trapping force Φ_z exerted on the particle in the trapped state, $(x_{\mathrm{col}}, y_{\mathrm{col}}) = (x_{\mathrm{tip}}, y_{\mathrm{tip}})$, $d = 0.1R$ as a function of the anchoring strength w_{sub}. The particle has planar anchoring with $w_{\mathrm{col}} = 22$.

colloidal crystals of different symmetries and lattice parameters can be first assembled and then released to the LC bulk. By repeating this, potentially new forms of reconfigurable structural organization can be obtained and used for scalable fabrication of novel mesoscopic materials. It will be of interest to extend our work to the colloidal nanoparticle regime, which may open new avenues for the design of new composite architectures for applications in nanophotonics, renewable energy, and plasmonics. For example, it has been shown recently [41] that the utility of up-conversion nanoparticles, which are of interest for various photoconversion applications, can be dramatically improved by placing them at the tips of metal pyramids, which is due to plasmonic nanofocusing effects. The dispersion of such up-conversion nanoparticles in LC cells with arrays of pyramids may allow for their targeted placement at the tips of the pyramids, thus,

allowing for the design of LC-mediated assembly of photoconversion nanostructures.

In conclusion, convex protrusions can efficiently trap colloidal particles with an unlike anchoring condition. The magnitude of this effective interaction is controlled by the anchoring and the size of the protrusion. Pyramidlike protrusions are able to target the defects that surround the colloidal particles, and trapping of particles is observed even for weak anchoring strengths at the substrate. Another very important factor, not discussed here and which will influence the 2D self-assembly, is the nematic-mediated interaction between the colloids themselves. Potentially, via a smart design of a template, e.g., commensurate with the symmetry of the interaction, the last may even enhance the 2D self-assembly. On the other hand, if the interaction is undesirable, its magnitude may be decreased by decreasing the anchoring strength of the colloidal surface, while preserving the trapping efficiency of a template (see the Supplemental Material, Fig. S1). Although many strategies for employing our templating approach along with bulk colloidal interactions can be developed depending on the need, the simplest one could utilize colloidal chains forming bulk crystals, similar to the 2D and 3D interparticle and intercolloidal-chain interactions reported in Refs. [16,18]. The pyramid, in this case, would act as end points of the colloidal chains nucleating their growth into the bulk, thus, defining the orientation of crystallographic axes.

N. M. S. and M. T. acknowledge financial support from the European Union via the FP7 Marie-Curie Grant No. PIRSES-GA-2010-269181. N. M. S. also acknowledges financial support from FCT Grants No. SFRH/BPD/40327/2007, No. EXCL/FIS-NAN/0083/2012, and No. PEstOE/FIS/U10618/2011. Q. L., B. S., and I. I. S. acknowledge the support of the DOE Grant No. ER46921.

*miko@is.mpg.de

[1] Y. Liu and X. Zhang, Chem. Soc. Rev. **40**, 2494 (2011).
[2] Y. Xia, B. Gates, Y. Yin, and Y. Lu, Adv. Mater. **12**, 693 (2000).
[3] O. Vickreva, O. Kalinina, and E. Kumacheva, Adv. Mater. **12**, 110 (2000).
[4] A. van Blaaderen, R. Ruel, and P. Wiltzius, Nature (London) **385**, 321 (1997).
[5] Y. D. Yin and Y. N. Xia, Adv. Mater. **14**, 605 (2002).
[6] Y. Xia and G. M. Whitesides, Angew. Chem., Int. Ed. **37**, 550 (1998).
[7] P. Poulin, H. Stark, T. C. Lubensky, and D. A. Weitz, Science **275**, 1770 (1997).
[8] T. C. Lubensky, D. Pettey, N. Currier, and H. Stark, Phys. Rev. E **57**, 610 (1998).
[9] S. Ramaswamy, R. Nityananda, V. A. Raghunathan, and J. Prost, Mol. Cryst. Liq. Cryst. **288**, 175 (1996).
[10] R. W. Ruhwandl and E. M. Terentjev, Phys. Rev. E **55**, 2958 (1997).
[11] J. C. Loudet and P. Poulin, Phys. Rev. Lett. **87**, 165503 (2001).
[12] M. Yada, J. Yamamoto, and H. Yokoyama, Phys. Rev. Lett. **92**, 185501 (2004).
[13] I. I. Smalyukh, O. D. Lavrentovich, A. N. Kuzmin, A. V. Kachynski, and P. N. Prasad, Phys. Rev. Lett. **95**, 157801 (2005).
[14] C. M. Noël, G. Bossis, A.-M. Chaze, F. Giulieri, and S. Lacis, Phys. Rev. Lett. **96**, 217801 (2006).
[15] J.-C. Loudet, P. Barois, and P. Poulin, Nature (London) **407**, 611 (2000).
[16] I. Muševič, M. Skarabot, U. Tkalec, M. Ravnik, and S. Žumer, Science **313**, 954 (2006).
[17] M. Tasinkevych, N. M. Silvestre, and M. M. T. da Gama, New J. Phys. **14**, 073030 (2012).
[18] A. Nych, U. Ognysta, M. Škarabot, M. Ravnik, S. Žumer, and I. Muševič, Nat. Commun. **4**, 1489 (2013).
[19] J. S. Lintuvuori, A. C. Pawsey, K. Stratford, M. E. Cates, P. S. Clegg, and D. Marenduzzo, Phys. Rev. Lett. **110**, 187801 (2013).
[20] M. A. Gharbi, M. Nobili, and C. Blanc, J. Colloid Interface Sci. **417**, 250 (2014).
[21] T. Lee, R. P. Trivedi, and I. I. Smalyukh, Opt. Lett. **35**, 3447 (2010).
[22] R. P. Trivedi, T. Lee, K. A. Bertness, and I. I. Smalyukh, Opt. Express **18**, 27658 (2010).
[23] P. G. de Gennes and J. Prost, *The Physics of Liquid Crystals* (Claredon, Oxford, 1993), 2nd ed.
[24] N. M. Silvestre, P. Patrício, and M. M. Telo da Gama, Phys. Rev. E **69**, 061402 (2004).
[25] I. I. Smalyukh, A. N. Kuzmin, A. V. Kachynski, P. N. Prasad, and O. D. Lavrentovich, Appl. Phys. Lett. **86**, 021913 (2005).
[26] Q. Xu, I. Tonks, M. J. Fuerstman, J. C. Love, and G. M. Whitesides, Nano Lett. **4**, 2509 (2004).
[27] J. B. Fournier and P. Galatola, Europhys. Lett. **72**, 403 (2005).
[28] See Supplemental Material at http://link.aps.org/supplemental/10.1103/PhysRevLett.112.225501, which includes Refs. [29–35], for the definition of Q_b and for the short description of the numerical approach.
[29] T. C. Lubensky, Phys. Rev. A **2**, 2497 (1970).
[30] F. C. Frank, Discuss. Faraday Soc. **25**, 19 (1958).
[31] M. Ravnik and S. Žumer, Liq. Cryst. **36**, 1201 (2009).
[32] R. Cools, J. Complexity **19**, 445 (2003).
[33] P. Keast, Comput. Methods Appl. Mech. Eng. **55**, 339 (1986).
[34] J. C. Gilbert and C. Lemaréchal, Math. Program. **45**, 407 (1989).
[35] J. Nocedal, Math. Comput. **35**, 773 (1980).
[36] S. Kralj, S. Žumer, and D. W. Allender, Phys. Rev. A **43**, 2943 (1991).
[37] M. Tasinkevych, N. M. Silvestre, P. Patrício, and M. M. T. da Gama, Eur. Phys. J. E **9**, 341 (2002).
[38] C. D. Modes, K. Bhattacharya, and M. Warner, Phys. Rev. E **81**, 060701(R) (2010).
[39] M. E. McConney, A. Martinez, V. P. Tondiglia, K. M. Lee, D. Langley, I. I. Smalyukh, and T. J. White, Adv. Mater. **25**, 5880 (2013).
[40] L. T. de Haan, C. Sánchez-Somolinos, C. M. W. Bastiaansen, A. P. H. J. Schenning, and D. J. Broer, Angew. Chem., Int. Ed. **51**, 12469 (2012).
[41] Q.-C. Sun, H. Mundoor, J. C. Ribot, V. Singh, I. I. Smalyukh, and P. Nagpal, Nano Lett. **14**, 101 (2014).